

Atomistic Simulation for Shallow Junction Formation

● Hideki Oka ● Kunihiro Suzuki ● Zhang Jinyu ● Min Yu
● Ru Huang

(Manuscript received January 30, 2003)

This paper presents an atomistic model for ion implantation and annealing to simulate shallow junction formation. In our code, the newest physical models are included and a great number of efficient algorithms are used to conduct realistic and accurate simulations. By comparing our simulation results with SIMS data for B and As ranging from 0.5 keV to more than 100 keV implantation, we verified the correctness and efficiency of our code. The annealing simulation is carried out for RTA (Rapid Thermal Annealing) at 1000°C or 1050°C after B implantation. The implantation energy was varied from 0.5 to 5 keV. Agreements between the simulations and SIMS data were achieved, and the simulations accurately characterized both BED and TED phenomena.

1. Introduction

With the scaling down of device size, ultra shallow junction technology becomes more and more important for the suppression of short channel effects, resulting in the requirement of lower energy ion implantation. Shallow junction formation requires a lower energy ion implantation, lower annealing temperature, and shorter annealing time.¹⁾ TED (Transient Enhanced Diffusion) and BED (Boron Enhanced Diffusion), which occur during high-temperature annealing such as RTA are barriers to the formation of shallow junctions.²⁾ Therefore, there is an urgent need to simulate BED as well as TED in TCAD (Technology CAD).

The atomistic model is recognized to be efficient and accurate because it includes the complex mechanism for ion implantation and diffusion simulations. Some good results from atomistic annealing simulation have been published.³⁾ The method has even been applied to the study of CMOS characteristics.⁴⁾ In this paper, we propose an atomistic model that characterizes both BED and TED. We simulated the RTA annealing at

1000°C and 1050°C after boron (B) implantation. The simulated implantation energy ranged from 0.5 keV to more than 100 keV. The simulation results were verified by SIMS (Secondary Ion-microprobe Mass Spectrometer) data. The model enables accurate simulations of both BED and TED, and we have achieved good agreements between experiments and simulations using this model. Our results suggest that the number of boron jumps are related to the enhancement of diffusion.

2. Atomistic model

2.1 Ion implantation

In the field of ion-solid interaction simulation, binary collision approximation (BCA) methods and molecular dynamics (MD) methods are both extensively used. BCA methods focus on the collisions between energetic ions and target atoms, calculating the asymptotic motion of ions and ignoring the correlation effects of neighboring atoms recoiling with each other. BCA is valid for high incident energies. However, BCA fails

when the collisions between recoiling atoms become significant or the time span within a collision event is larger for the calculation of asymptotic trajectories, for example, in the case of channeling implantation. Compared with BCA, MD methods provide a clearer insight into the ion-target collisions, because they deal with the interactions between ions and atoms as well as among atoms themselves. Using MD methods, the forces are obtained from the analytical derivative of the potential function. Then, the trajectories of ions and atoms are derived by numerically integrating the Newtonian equation. Although MD simulations consume more computing time and require more powerful computing facilities, they have recently become feasible thanks to the rapid enhancement of computing ability, the development of more efficient algorithms, and the fact that low-energy ion implantation requires fewer calculations.

2.2 Models and algorithms

2.2.1 Models

The slowing down of incident ions in solids is mainly caused by two mechanisms: 1) elastic collisions of energetic ions with atoms and 2) collisions between the ions and electrons. An accurate description of these interactions is therefore the key to obtaining realistic simulation results.

- **Ion-target**

The ZBL universal potential,⁵⁾ which is based on the numerical average of many potential functions, is generally used and usually provides sufficient accuracy. However, if there is a large difference between the real potential and the numerical average, using the ZBL universal potential causes a large error. In this paper, therefore, we describe the interactions between ions and atoms using the DMol potential, which is calculated from density function theory and believed to be more accurate than the ZBL universal potential.⁶⁾

- **Target-target**

For the interactions between target atoms,

we use the Stillinger-Weber many-body potential description.⁷⁾

- **Ion-electron**

We have implemented the local electronic stopping model proposed by Cai et al.⁸⁾ and the Firsov model⁹⁾ in our code to describe energy losses in inelastic collisions of incident ions with target atoms. Cai's model is based on the Brandt-Kitagawa theory and has only one fitting parameter, r_s^0 . The electronic stopping power of an ion contains two components: the effective charge, Z_{eff} , and the charge density dependent electronic stopping power for a proton, S_p . The electronic stopping, S_e , can be defined as:⁸⁾

$$S_e = Z_{eff}^2(v_1, r_s^0) S_p(v_1, r_s) \quad (1)$$

where v_1 is the reduced relative velocity of the ion and r_s is the one-electron density ($r_s = (3/4\pi\rho)^{1/3}$, where ρ is the local electron density).

- **Inelastic energy loss**

The Firsov model is used to describe the energy loss of an ion due to inelastic collisions with target atoms. This is a velocity-dependent potential, and the force between atom i and j is:

where

$$\mathbf{F}_{ij} = \frac{2^{1/3}\eta}{2\pi a_B^2} (\mathbf{v}_j - \mathbf{v}_i) \left[Z_1^2 I \left(\frac{Z_1^{1/3} \alpha R}{a} \right) + Z_2^2 I \left(\frac{Z_2^{1/3} (1 - \alpha) R}{a} \right) \right] \quad (2)$$

$$I(X) = \int_x^\infty \frac{\phi^2(x)}{x} dx, \quad \alpha = \left[1 + \left(\frac{Z_2}{Z_1} \right)^{1/6} \right]^{-1} \quad (3)$$

and a_B is the Bohr radius, Z is the atomic number ($Z_1 > Z_2$), R is the distance between two atoms, and $a = (9\pi^2/128)^{1/3} a_B$. $\phi(x)$ is a screening function. We used a ZBL-type expression⁵⁾ in our program:

$$\phi(x) = 0.1818e^{-3.2x} + 0.5099e^{-0.9423x} + 0.2802e^{-0.4029x} + 0.02817e^{-0.2016x} \quad (4)$$

The electronic stopping and the inelastic energy loss are two different mechanisms. They play different roles under different conditions, and neither of them can be ignored in most cases, especially in channeling implantation.

All of the above models are integrated in a molecular dynamics code that we have developed called LEACS (Low Energy Atomic Collision Simulation)¹⁶⁾ to simulate low-energy ion implantation. Most of the simulation parameters can be switched on or off to include or exclude physical effects such as the interactions between target atoms, electronic stopping, inelastic energy losses, surface amorphization, and lattice vibration, depending on the specific cases of implantation.

2.2.2 Approximations and algorithms

Despite the condition of low implantation energy, full MD simulation methods are still too time-consuming. Hence, a lot of approximations have to be introduced into our simulation. RIA (Recoil Interaction Approximation) methods,¹⁰⁾ which only deal with the interactions between ions and target atoms, have proved to be very successful for calculating the range profile. Interactions between target atoms will have some influence on the tail of the range, but less influence on other parts. On the other hand, calculating the interactions between target atoms will consume a great deal of time, so when the details of the profile's tail are not very important, we can switch that calculation off.

To obtain a good accuracy over at least three orders of concentration magnitude in a short time, we also introduce the rare-event algorithm (REA).¹¹⁾

For low-dose implantation, the correlation between different incident ions is small, so we can ignore the cascade damage caused by the previous incident ions. By using the moving-box method,¹⁰⁾ a simulation box of only $3 \times 3 \times 3$ unit cells (about 200 atoms) is needed, which saves a lot of memory. Every time the ion moves closer than R_s (a pre-defined separation) to the box border, the simulation box needs to be updated. R_s is usually equal to the size of the unit cell, which is equal to the lattice constant.

For the simulations presented here, the target is {100}Si with a 10 Å surface amorphous oxide

layer. Our code can also support a multi-layer structure which consists of a crystalline layer such as a Si or Ge layer and a non-crystalline layer such as an SiO₂ or Si₃N₄ layer. The thermal vibrations of lattice atoms are described using the Debye model. The Debye temperature for Si is 5190 K.¹³⁾ The target temperature is 300 K. A beam divergence of 1° was assumed. The fitting parameter, r_s^0 , for the electronic stopping model is set to 1.217 Å for boron, phosphorus, and arsenic.

2.3 Annealing simulator

A simulator called the AMAS (Atomistic Model Annealing Simulator) has been developed based on the Kinetic Monte Carlo model (KMC).¹⁴⁾

In order to simulate the annealing process for ion implantation, a box that contains all the necessary ions and damages is defined. For implantation, the concentration profile is even in the lateral direction, which is perpendicular to the direction of implantation, except at the edge of the implanted field. We only simulate the field in the center of the implantation window. The width of the simulation box is much smaller than that of the implantation window. Thus, the periodical boundary is applied to the box in the lateral direction. Reducing the box size can considerably reduce the computing time. However, the box length should be set carefully so that the box is long enough for diffusion simulation and the required computation time is acceptable. At the same time, an orthogonal mesh is constructed in the box to divide the box into many small cells. Each side of a cell is 2.34 Å long so that the cell takes up the average volume occupied by an atom in crystal silicon. The mesh is introduced mainly to simplify the calculations for finding neighboring particles. All of the particles in the box can be mapped onto the mesh. Therefore, the neighboring particles can be found by checking the contents of neighboring cells instead of calculating the distances between all the particles.

Particles defined in the model are single particles and clusters. Single particles are dopants

and point defects. The lattice silicon atoms are excluded so that the total number of particles in the system and the computing time can be greatly reduced. The entire lattice of silicon is treated as the background of the simulated area. In this paper, only boron implantation is studied, because it was the only dopant in our experiments. Point defects include silicon interstitials (I) and lattice vacancies (V). Clusters, including silicon interstitial clusters (I_n), vacancy clusters (V_n), and boron silicon complexes (B_nI_m), are defined as the compounds of single particles. The possible particle events are migration, annihilation, and combination and evaporation of clusters. Migration means the movement of mobile particles such as I , V , and interstitial boron pairs (B). Annihilation means annihilation between V and I . Combination means the creation and growth of clusters. Evaporation means the evaporation of clusters by the emission of single particles. The combination actions of clusters are as follows:

$$I_n + I \Leftrightarrow I_{n+1} \tag{5}$$

$$V_n + V \Leftrightarrow V_{n+1} \tag{6}$$

$$B_nI_m + Bi \Leftrightarrow B_{n+1}I_{m+1} \tag{7}$$

$$B_nI_m + I \Leftrightarrow B_nI_{m+1} \tag{8}$$

where, for I_n and V_n , $n < 100$ and for B_nI_m , $n < 5$ and $m < 5$. Migration and evaporation happen at a rate determined by the energy barrier, E_b :

$$v = v_0 \exp\left(\frac{-E_b}{KT}\right) \tag{9}$$

where E_b is the migration energy barrier for a migration event or the binding energy for cluster evaporation. v_0 is the attempt frequency and is generally set to about $10^{13}/s$, depending on the thermal oscillation frequency of the atoms. The basic parameters used for simulation are shown in **Table 1**.

The binding energy of I_n is $2.0 - 1.95(n^{1/2} - (n - 1)^{1/2})$ and that of V_n is $2.5 - 2.8(n^{2/3} - (n-1)^{2/3})$ in eV units. n is the size of the cluster. The value

Table 1
Main parameters for simulation.

Events	v_0 ($10^{15}/s$)	E_b (eV)
V migration	0.0025	0.45
I migration	0.01	0.9
Bi migration	0.01	0.3
$BI = B + I$	0.01	0.6

of parameter n in these two expressions is obtained by fitting theoretical data and experimental results.¹⁴⁾ The binding energy of B_nI_m can be calculated from the total energy scheme presented by Pelaz.³⁾ The Cluster model is important in explaining TED phenomenon.³⁾ Annihilation and combination are assumed to occur whenever two concerned particles are close enough to each other. The interactions between particles are so fast that they take up a negligible amount of computing time.

BED is thought to be caused by the emission of Si interstitials from the surface.¹⁵⁾ However, there is still disagreement about the source of these emissions. On the other hand, it has been suggested that surface emission should also be considered for TED.¹⁵⁾ To accurately simulate both BED and TED, we use a surface emission model in the simulator. Although boride may be the source of Si interstitials, our simulator does not have a special model for boride. In our model, the surface is treated as a source and sink for point defects. Defects are trapped at the surface, and surface emissions occur at the same time. Point defects emitted from the surface are point defects that were previously trapped by the surface. Thus, only defects that are generated in implantation are included. As a simple approximation, the rate of surface emission equals that of annihilation.

3. Results and discussion

3.1 Ion implantation

To verify the simulator, we have compared the simulated results with SIMS data for different cases. The energy range of simulations is from

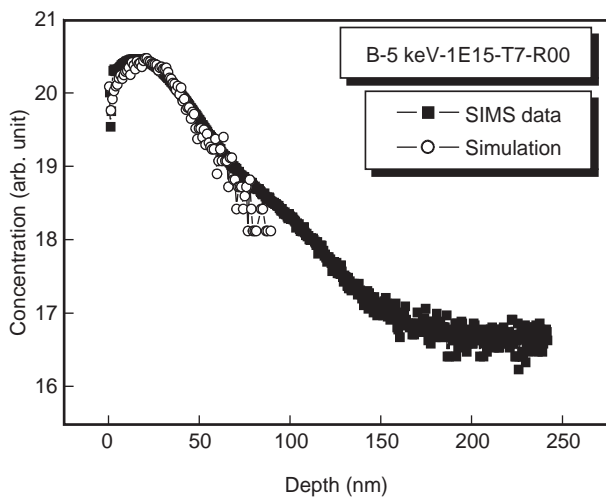


Figure 1
Range profile of 5 keV boron (7,0) implantation into (100) Si with $1E15 \text{ cm}^{-2}$ dose.

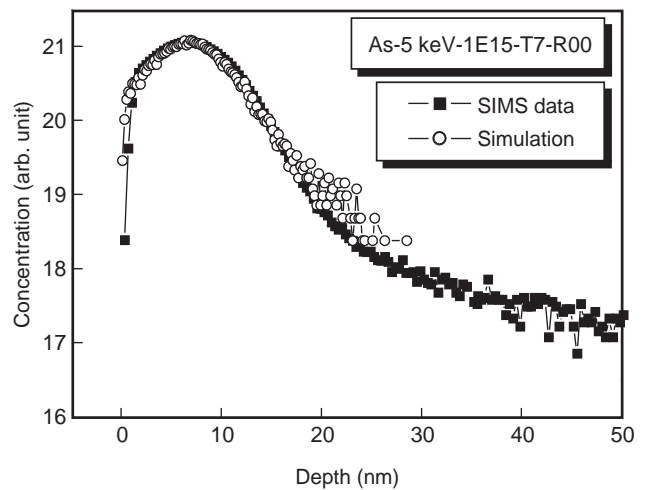


Figure 3
Range profile of 5 keV arsenic (7,0) implantation into (100) Si with $1E15 \text{ cm}^{-2}$ dose.

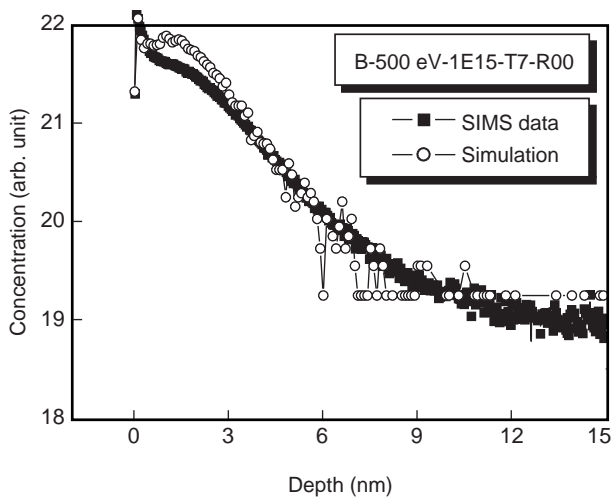


Figure 2
Range profile of 500 eV boron (7,0) implantation into (100) Si with $1E15 \text{ cm}^{-2}$ dose.

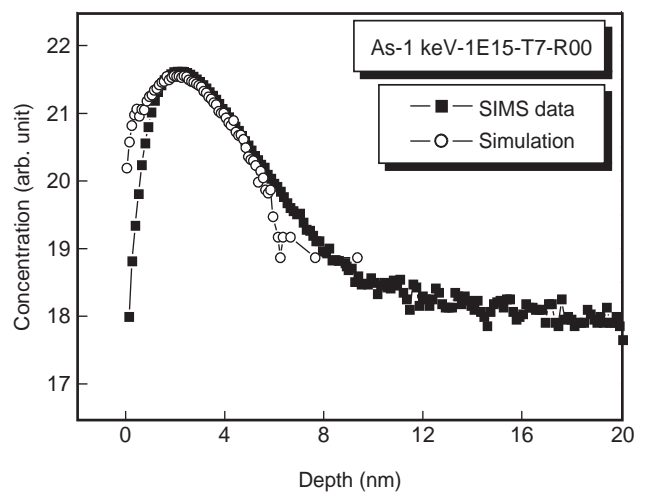


Figure 4
Range profile of 1 keV arsenic (7,0) implantation into (100) Si with $1E15 \text{ cm}^{-2}$ dose.

0.5 to 5 keV for boron and from 1 to 5 keV for arsenic. The dose range of simulations includes $5E12 \text{ cm}^{-2}$, $5E13 \text{ cm}^{-2}$, $5E14 \text{ cm}^{-2}$, and $1E15 \text{ cm}^{-2}$ for boron and arsenic. The implantation condition is a non-channeling condition (tilt and rotation angles are 7° and 0° , respectively). **Figures 1 to 4** show that the simulator is accurate enough in the peak region for all cases. Especially, the simulator has successfully predicted the position and the

peak concentration, which are the main features of a range profile. The shape of the simulated results also agree with that of SIMS data, except in cases of low-dose or low-energy boron. However, SIMS data itself is not reliable in those cases because the SIMS instrument's resolving power is limited.

In high-dose and high-energy cases, there are insufficient points to cover the tail of the range

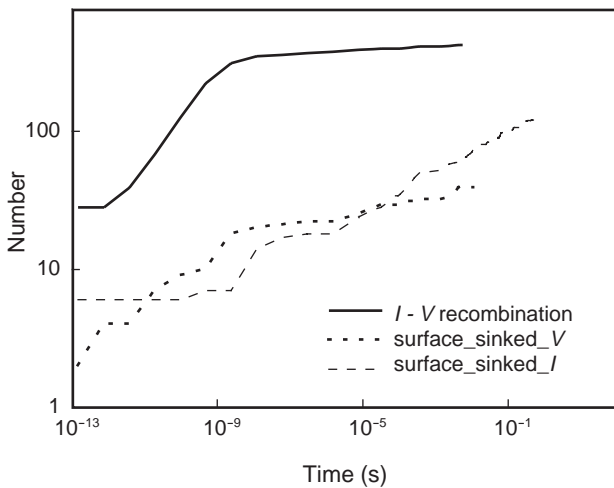


Figure 5 Simulated annihilation of point defects during 800°C annealing. *I* indicates silicon interstitials, and *V* indicates vacancies.

profile. However, the range profile has an effective region whose area is proportional to the dose. Also, all of the simulated results just cover the effective regions. Thus, the simulated curves are thought to be effective.

3.2 Annealing

To study the characteristics of silicon intrinsic defects, we performed an annealing simulation at 800°C. We used a box of about 80×80×550 Å³ containing only silicon interstitials and vacancies. The initial distribution of defects was taken to be Gaussian, with the peak position at 50 Å from the surface. We also conducted a boron annealing simulation using a box of about 100×100×550 Å³. The initial distribution needed by KMC (Kinetic Monte Carlo) was generated using our LEACS¹⁶⁾ MD implantation simulator.

3.2.1 The annihilation of defects

When annealing starts, the *I* (silicon interstitials) and *V* (vacancies) defects move in random directions. They may recombine with each other or sink at the surface. A simulation of the number of recombined and sunken defects during annealing is shown in **Figure 5**.

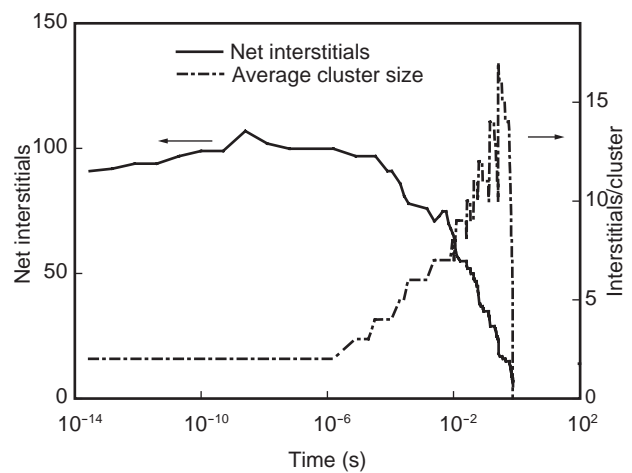


Figure 6 Simulated Ostwald ripening of interstitial clusters during 800°C annealing. Ostwald ripening is also observed in experiments.¹⁷⁾

It can be seen that the recombination of *I* and *V* mainly occurs in the early stage of annealing. After 10⁻⁸ seconds, this process slows down, because the density of defects decreases significantly. This is inconsistent with the simulation result of M. Jaraiz.¹⁴⁾

3.2.2 The Ostwald ripening of clusters

During annealing, point defects may gather into clusters in a process called Ostwald ripening. A simulation of Ostwald ripening of interstitial clusters is shown in **Figure 6**.

The net interstitials are the number of *I* minus the number of *V*. The figure shows that the clusters undergo a ripening process, during which they increase in size and then evaporate. This phenomenon is also observed in experiments.¹⁷⁾

Figure 7 shows a simulation of Ostwald ripening in more detail. Initially, there are many small clusters, but then many of them evaporate during annealing so that the number rapidly decreases. The free interstitials emitted by clusters wander about. Some of them are recaptured by clusters, while others are annihilated at the surface. Some of the clusters expand by capturing free interstitials. As a result, the average size of

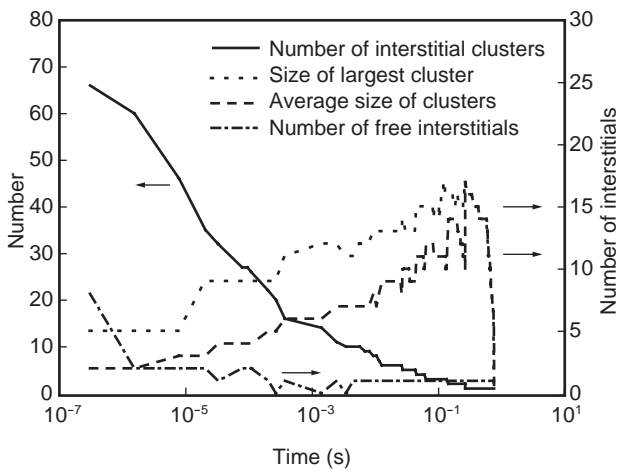


Figure 7
Simulated Ostwald ripening of interstitial clusters during 800°C annealing.

clusters and the size of the largest cluster increase with time. One possible explanation for Ostwald ripening is that the binding energy of clusters increases with size so that the larger clusters are less likely to evaporate than the smaller ones. The smaller clusters evaporate first and give out free interstitials, and at the same time the bigger clusters get chances to expand.

3.2.3 Simulation of TED

We used our LEACS¹⁶⁾ MD simulator to simulate RTA after 5 keV boron implantation to verify whether it causes TED. The implantation energy was varied from 13 to 0.5 keV. The coordinates of all point defects and dopants were imported into AMAS.

The results are shown in **Figure 8**. In this case, there was good agreement between the simulation and SIMS data and the occurrence of TED is obvious.

In order to study the ability to simulate immobile peak phenomenon in TED, we simulated annealing for 5 keV at a different dose. The results are shown in **Figure 9**. As the figure shows, unlike the case for 5 keV and $1E15\text{ cm}^{-2}$, there is an obvious immobile peak after annealing for 5 keV and $2E15\text{ cm}^{-2}$.

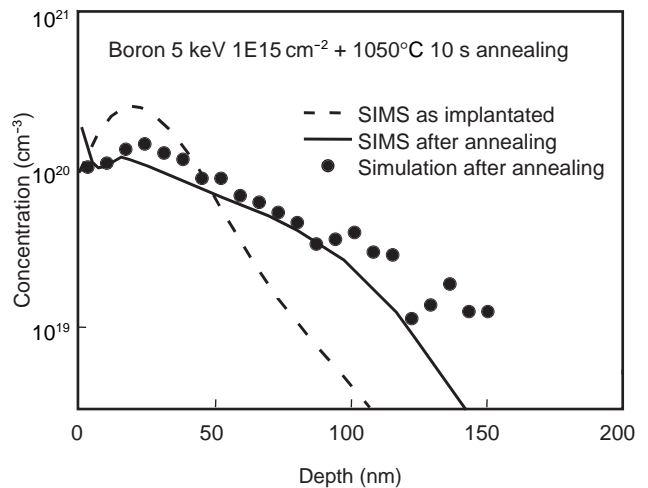


Figure 8
Simulated RTA after boron implantation at $1E15\text{ cm}^{-2}$.

3.2.4 Simulation of BED

It is reported in Ref. 2) that, using SIMS, BED was experimentally found to occur in boron implantation performed at very low energies. We therefore simulated the reported SIMS experiment by AMAS to verify if the model is valid for BED. The reported SIMS results were for samples annealed after 0.5 keV implantation. The results are shown in **Figure 10**.

The figure shows there is a close agreement between the SIMS and simulated results. We can therefore conclude that the model is capable of simulating BED. All the parameters used here were the same as those used in the TED simulation described above. Thus, the model is valid for both TED and BED simulations.

4. Conclusions

In this paper, we presented our computer simulations of low-energy ion implantation using an MD simulator we have developed. We included the newest physical models on nuclear stopping and electronic stopping and implemented many efficient algorithms in our program. The code also considers the effects of surface amorphization. Our simulation results agree very well with experimental data for boron and arsenic implants.

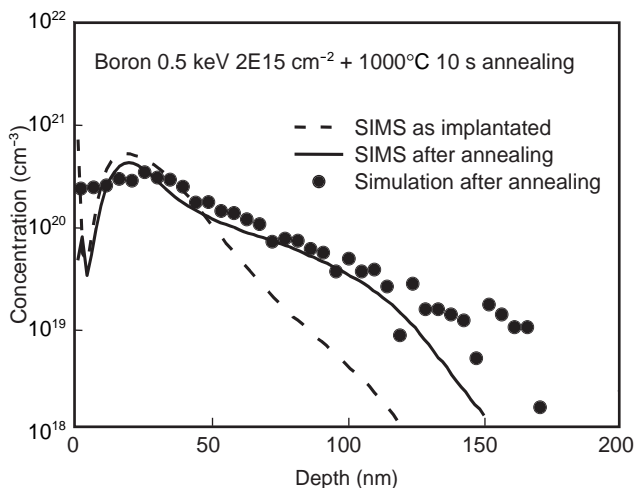


Figure 9
Simulated RTA after boron implantation at $2E15 \text{ cm}^{-2}$. Note the post-annealing peak.

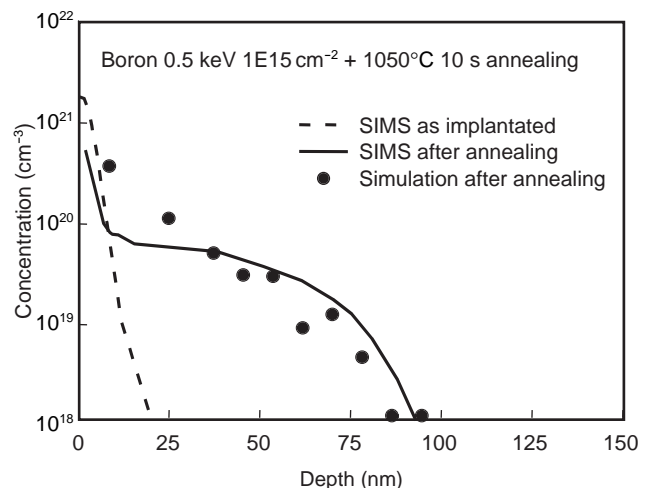


Figure 10
Simulation of annealing experiments reported in Ref. 2), in which the BED phenomenon is identified. Note the close agreement between the SIMS and simulated results.

For all cases, only one fitting parameter is needed, leading to a large reduction of operating complexity.

We also presented the results of annealing simulations we conducted using a KMC-based atomistic model we developed. We found that the recombination of interstitials and vacancies mainly occurs in the early stage of annealing. Interstitial clusters undergo Ostwald ripening, which has been found to occur in experiments. Our simulator can provide the density profile of boron after annealing, and it accurately simulates TED and BED, which are critical points in shallow junction formation. The results indicate that an atomistic model is feasible in annealing process simulation and can provide detailed information about the evolution of all defects and dopants in ultra shallow junction formation.

Acknowledgements

We thank Dr. Hideaki Fujitani from Fujitsu Laboratories Ltd. and Dr. Andrew P. Horsfield from the Fujitsu European Center for Information Technology for their cooperation at the early stage of this work. We also thank Dr. L. Pelaz, M. Jaraiz, and Dr. P. Castrillo-Romon from the

University of de Valladolid, Spain for the very helpful discussions we had with them.

References

- 1) V. Raineri, R. J. Schreutelkamp, F. W. Saris, R. E. Kaim, and K. T. F. Janssen: Secondary defect reduction by channeling implantation of B and P in $\langle 100 \rangle$ silicon. *Nucl. Instr. Meth. Phys. Res.*, **B 59/60**, p.1056 (1991).
- 2) Aditya Agarwal, D. J. Eaglesham, H. J. Gossmann, Lourdes Pelaz, S. B. Herner, D. C. Jacobson, T. E. Haynes, Y. Erokhin, and R. Simonton: Boron-enhanced-diffusion of boron: The limiting factor for ultra-shallow junctions. *IEDM*, p.467 (1997).
- 3) Lourdes Pelaz, G. H. Gilmer, H. J. Gossmann, C. S. Rafferty, M. Jaraiz, and J. Barbolla: B cluster formation and dissolution in Si: A scenario based on atomistic modeling. *Appl. Phys. Lett.*, **74**, 24, p.3657 (1999).
- 4) M. Hane, T. Ikezawa, K. Takeuchi, and G. H. Gilmer: Monte Carlo impurity diffusion simulation considering charged species for low thermal budget sub-50 nm CMOS process modeling. *IEDM*, 2001.
- 5) J. F. Ziegler, J. P. Biersack, and U. Littmark:

- The Stopping and Range of Ions in Matter. Pergamon. New York, 1985.
- 6) K. Nordlund, N. Runeberg, and D. Sundholm: Repulsive interatomic potentials calculated using Hartree-Fock and density-functional theory methods. *Nucl. Instr. Meth. Phys. Res.*, **B132**, p.45 (1997).
 - 7) F. H. Stillinger and T. A. Weber: Computer simulation of local order in condensed phases of silicon. *Phys. Rev.*, **B31**, p.5262 (1985).
 - 8) D. C. Charles, M. Snell, K. M. Beardmore, and N. G.-Jensen: Simulation of phosphorous implantation into silicon with a single parameter electronic stopping power model. *Int. J. Mod. Phys. C.*, **9**, p.459 (1998).
 - 9) O. B. Firsov, *Sov. Phys. JETP*, **36**, 9, p.1076 (1959).
 - 10) K. Nordlund: Molecular dynamics simulation of ion ranges in the 1-100 keV energy range. *Comput. Mater. Sci.*, **3**, p.448 (1995).
 - 11) K. Beardmore and N. G.-Jensen: Efficient molecular dynamics scheme for the calculation of dopant profiles due to ion implantation. *Phys. Rev.*, **E 57**, p.7278 (1998).
 - 12) L. Verlet: Computer experiments on classical fluids. I. Thermodynamical properties of Lennard-Jones molecules. *Phys. Rev.*, **159**, p.98 (1967).
 - 13) G. Buschhorn, E. Diedrich, W. Kufner, M. Rzepka, H. Genz, P. H.-Stascheck, and A. Richter: Temperature dependence of planar channeling radiation in silicon, germanium, and beryllium between 12 and 300 K. *Phys. Rev.*, **B55**, p.6196 (1997).
 - 14) M. Jaraiz, G. H. Gilmer, J. M. Poate, and T. D. de la Rubia: Atomistic calculation of ion implantation in Si: point defect and transient enhanced diffusion phenomena. *Appl. Phys. Lett.*, **68**, 3, p.409 (1996).
 - 15) N. E. B. Cowern, M. J. J. Theynissen, F. Roozeboom, and J. G. M. van Berkum: Boride-enhanced diffusion in silicon: Bulk and surface layers. *Appl. Phys. Lett.*, **75**, 2, p.181 (1999).
 - 16) R. Yajun, G. Wenyu, H. Ru, Y. Min, Z. Xing, and W. Yangyuan: Computer simulation on low energy ion implantation based on molecular dynamics methods. *Chinese Journal of Electronics*, **9**, p.359 (2000).
 - 17) D. J. Eaglesham, P. A. Stolk, H.-J. Gossmann, and J. M. Poate: Implantation and transient B diffusion in Si: the source of the interstitials. *Appl. Phys. Lett.*, **65**, 18, p.2305 (1994).



Hideki Oka received the B.S. and M.S. degrees in Solid State Physics from the University of Tokyo, Tokyo, Japan in 1973 and 1975, respectively. He joined Fujitsu Laboratories Ltd., Kawasaki, Japan in 1975. He also worked in Cray Research, Silicon Graphics, and Main-gate Electronics Ltd. He rejoined Fujitsu Laboratories Ltd. Atsugi, Japan in 2000. His main research interests

are simulation technologies for advanced semiconductor processes and devices and high-performance computing technologies. He is a member of the IEICE, JSAP, and IEEE.

E-mail: oka.hideki@jp.fujitsu.com



Min Yu received the B.S. degree in Material Physics and the M.S. degree in Condensed State Physics from Beijing Normal University, P. R. of China in 1996 and 1999, respectively. He joined Peking University in 1999. His research interests are semiconductor devices and processes. He is currently engaged in atomistic process simulation.



Ru Hunag received the B.S. (highest honors) and M.S. degrees in Electronic Engineering from Southeast University, Nanjing, China in 1991 and 1994 and the Ph.D. degree from Peking University, Beijing, China in 1997. She joined the Institute of Microelectronics, Peking University in 1997 and became an associate professor in 1999. Her main research interests are SOI technologies, deep sub-micron device technologies,

novel device structures and processing, device modeling, low-energy implantation simulation, and RF circuits.



Kunihiro Suzuki received the B.S., M.S., and Ph.D. degrees in Electronics Engineering from the Tokyo Institute of Technology, Tokyo, Japan in 1981, 1983, and 1996, respectively. He joined Fujitsu Laboratories Ltd., Atsugi, Japan in 1983, where he has been engaged in design and modeling of high-speed bipolar and MOS transistors. He was a visiting researcher at the Swiss Federal Institute of Technology (ETH) Zurich,

Switzerland in 1996 and 1997, where he studied process modeling. His current interests are process and device modeling. He is a senior member of the IEEE.

E-mail: suzuki.kunihiro@jp.fujitsu.com



Zhang Jinyu received the B.S., M.S., and Ph.D. degrees in Physics from Tsinghua University, Beijing, China in 1993, 1995, and 1998, respectively. He joined the Fujitsu Research and Development Center in 1998, where he has been engaged in atomic device and process simulation.